Monthly Notices
of the
ROYAL ASTRONOMICAL SOCIETY

MNRAS **464,** 1493–1501 (2017)
Advance Access publication 2016 September 30

doi:10.1093/mnras/stw2495

The clustering of galaxies in the completed SDSS-III Baryon Oscillation Spectroscopic Survey: combining correlated Gaussian posterior distributions

Ariel G. Sánchez,[1⋆] Jan Niklas Grieb,[1,2] Salvador Salazar-Albornoz,[1,2] Shadab Alam,[3,4] Florian Beutler,[5,6] Ashley J. Ross,[5,7] Joel R. Brownstein,[8] Chia-Hsun Chuang,[9,10] Antonio J. Cuesta,[11] Daniel J. Eisenstein,[12] Francisco-Shu Kitaura,[6,10,13] Will J. Percival,[5] Francisco Prada,[8,14,15] Sergio Rodríguez-Torres,[8,14,16] Hee-Jong Seo,[17] Jeremy Tinker,[18] Rita Tojeiro,[19] Mariana Vargas-Magaña,[3,4,20] Jose A. Vazquez[21] and Gong-Bo Zhao[5,22]

Affiliations are listed at the end of the paper

Accepted 2016 September 29. Received 2016 September 28; in original form 2016 July 11

ABSTRACT

The cosmological information contained in anisotropic galaxy clustering measurements can often be compressed into a small number of parameters whose posterior distribution is well described by a Gaussian. We present a general methodology to combine these estimates into a single set of consensus constraints that encode the total information of the individual measurements, taking into account the full covariance between the different methods. We illustrate this technique by applying it to combine the results obtained from different clustering analyses, including measurements of the signature of baryon acoustic oscillations and redshift-space distortions, based on a set of mock catalogues of the final SDSS-III Baryon Oscillation Spectroscopic Survey (BOSS). Our results show that the region of the parameter space allowed by the consensus constraints is smaller than that of the individual methods, highlighting the importance of performing multiple analyses on galaxy surveys even when the measurements are highly correlated. This paper is part of a set that analyses the final galaxy clustering data set from BOSS. The methodology presented here is used in Alam et al. to produce the final cosmological constraints from BOSS.

Key words: cosmological parameters – large-scale structure of Universe.

1 INTRODUCTION

Over the past decades, the size and quality of galaxy redshift surveys have increased dramatically. Thanks to these data sets, the information from the large-scale structure (LSS) of the Universe has played a central role in establishing the current cosmological paradigm, the Λ cold dark matter (ΛCDM) model (e.g. Tegmark et al. 2004; Cole et al. 2005; Eisenstein et al. 2005; Anderson et al. 2012, 2014a,b).

Several methods can be used to extract the information encoded in the large-scale distribution of galaxies. The power spectrum, $P(k)$, and its Fourier transform, the two-point correlation function $\xi(s)$, have been the preferred tools for LSS analyses. The anisotropies in these measurements caused by redshift-space distortions (RSD) and the Alcock–Paczynski effect (Alcock & Paczynski 1979) can be studied by means of their Legendre multipoles (e.g. Padmanabhan & White 2008) or by using the clustering wedges statistic (Kazin, Sánchez & Blanton 2012). Thanks to the combined information of baryon acoustic oscillations (BAO) and RSD, anisotropic clustering measurements can simultaneously constrain the expansion history of the Universe and the growth of density fluctuations, thus offering one of the most powerful cosmological probes.

The potential of LSS observations as cosmological probes has led to the construction of increasingly larger galaxy catalogues. Examples of these surveys include the Two-degree Field Galaxy Redshift Survey (2dFGRS, Colless et al. 2001, 2003), the 6dF Galaxy Survey (6dFGS, Jones et al. 2009), the WiggleZ Dark Energy Survey (Drinkwater et al. 2010), the completed Baryon Oscillation Spectroscopic Survey (BOSS; Dawson et al. 2013), which is part of the Sloan Digital Sky Survey III (SDSS-III; Eisenstein et al. 2011), the ongoing SDSS-IV extended Baryon Oscillation Spectroscopic

⋆ E-mail: arielsan@mpe.mpg.de

Survey (eBOSS; Dawson et al. 2016), and future surveys such as the Hobby Eberly Telescope Dark Energy Experiment (HETDEX; Hill et al. 2008), the Dark Energy Spectroscopic Instrument (DESI; Levi et al. 2013) and the ESA space mission *Euclid* (Laureijs et al. 2011).

As the construction of galaxy surveys requires a considerable amount of resources from the community, substantial efforts are put into maximizing the information extracted from the obtained data sets. This problem has often been posed as that of determining which statistic is the best to extract cosmological information (e.g. power spectrum versus correlation function), often based on a simple metric or a figure of merit. However, although the results obtained by applying different statistics to a given data set are highly correlated, as they are based on estimators and each measurement is analysed over a limited range of scales, they do not contain exactly the same information or are affected by noise in the same way. This means that, if the covariance between the different measurements is correctly taken into account, additional information could be obtained by combining the results inferred from different methods.

In most cases, the cosmological information contained in the clustering measurements can be condensed into a small number of parameters whose posterior distribution is well described by a multivariate Gaussian. In this case, the obtained constraints can be represented by the mean values of these parameters and their respective covariance matrices. The analyses of the final BOSS galaxy samples of our companion papers are examples of this situation (Beutler et al. 2016a,b; Grieb et al. 2016; Ross et al. 2016; Sánchez et al. 2016; Satpathy et al. 2016). The BAO and RSD information obtained in these analyses can be expressed as constraints on the ratio of the comoving angular diameter distance to the sound horizon at the drag redshift, $D_{\rm M}(z)/r_{\rm d}$, the product of the Hubble parameter and the sound horizon, $H(z) \times r_{\rm d}$, and the growth rate of cosmic structures, characterized by the combination $f\sigma_8(z)$, where $f(z)$ is the logarithmic growth rate and $\sigma_8(z)$ represents the linear rms mass fluctuation in spheres of radius $8\,h^{-1}$ Mpc.

Here, we present a general methodology to combine several Gaussian posterior distributions into a single set of consensus constraints representing their joint information, taking into account the full covariance between the different estimates. We illustrate this technique by applying it to the results inferred from the application of the same clustering analyses performed on the final BOSS galaxy samples to 996 MULTIDARK-PATCHY (MD-PATCHY) mock galaxy catalogues, reproducing the properties of the survey (Kitaura et al. 2016). The obtained consensus distributions represent a gain in constraining power with respect to the results of the individual methods, highlighting the importance of performing multiple analyses on galaxy surveys. The methodology presented here is used in our companion paper Alam et al. (2016) to combine the cosmological information from the different analysis methods applied to the final BOSS galaxy samples (Beutler et al. 2016a,b; Grieb et al. 2016; Ross et al. 2016; Sánchez et al. 2016; Satpathy et al. 2016) into a final set of consensus constraints.

The structure of the paper is as follows. In Section 2, we present the general scheme for the combination of different Gaussian posterior distributions into a set of consensus constraints that encode the full information provided by these estimates. We consider the cases in which the posterior distributions cover the same parameter spaces and when they differ. In Section 3, we illustrate this procedure by applying it to the results obtained from different BAO and RSD measurements from a set of BOSS mock catalogues. Finally, Section 4 contains our main conclusions.

2 THE COMBINATION OF GAUSSIAN POSTERIOR DISTRIBUTIONS

In this section, we describe the general formalism to combine the information from several posterior distributions into a set of consensus constraints that fully account for their covariance. We begin with the case in which all distributions contain the same parameters and later extend these results to the more general case in which the overlap can be partial.

2.1 The combination of posterior distributions on the same parameter space

Let us assume that m different statistical analyses have been performed on a given data set, each of them producing an estimate of the same set of p parameters. If the posterior distributions of these parameters are well described by a Gaussian, the results of any given method i can be represented by an array of p measurements $\mathbf{D}_i$ and their corresponding $p \times p$ covariance matrix $\mathbf{C}_{ii}$. Considering all m methods, the full set of measurements can be written in a single array of dimension $m \times p$ as

$$\mathbf{D}_{\rm tot} = (\mathbf{D}_1, \cdots, \mathbf{D}_m)^{\rm t}, \tag{1}$$

with a total covariance matrix

$$\mathbf{C}_{\rm tot} = \begin{pmatrix} \mathbf{C}_{11} & \cdots & \mathbf{C}_{1m} \\ \vdots & \ddots & \vdots \\ \mathbf{C}_{m1} & \cdots & \mathbf{C}_{mm} \end{pmatrix}, \tag{2}$$

where each block $\mathbf{C}_{ij}$ represents the cross-covariance matrix between the results of methods i and j.

A given model will predict values for these parameters, which we will represent by the array $\mathbf{T}$. Defining

$$\mathbf{T}_{\rm tot} = (\mathbf{T}, \cdots, \mathbf{T})^{\rm t}, \tag{3}$$

that is, $\mathbf{T}$ repeated m times, and a total precision matrix as

$$\Psi_{\rm tot} \equiv \mathbf{C}_{\rm tot}^{-1}, \tag{4}$$

we can compute the χ^2 of a model, taking into account the combined information of all measurements, as

$$\chi^2 = (\mathbf{D}_{\rm tot} - \mathbf{T}_{\rm tot})^{\rm t} \Psi_{\rm tot} (\mathbf{D}_{\rm tot} - \mathbf{T}_{\rm tot}). \tag{5}$$

Our goal is to compress the combined information of all the measurements into a single set of p consensus values, $\mathbf{D}_{\rm c}$, with its corresponding $p \times p$ covariance matrix, $\mathbf{C}_{\rm c}$, such that

$$\chi^2_{\rm c} = (\mathbf{D}_{\rm c} - \mathbf{T})^{\rm t} \Psi_{\rm c} (\mathbf{D}_{\rm c} - \mathbf{T}), \tag{6}$$

where

$$\Psi_{\rm c} = \mathbf{C}_{\rm c}^{-1} \tag{7}$$

is equal to the χ^2 value of equation (5) up to an additive constant, which would only correspond to a renormalization of the likelihood function. In order to do this, we first write the full precision matrix, $\mathbf{\Psi}_{\rm tot}$, in blocks of size $p \times p$ as

$$\Psi_{\rm tot} = \begin{pmatrix} \mathbf{\Psi_{11}} & \cdots & \mathbf{\Psi}_{1m} \\ \vdots & \ddots & \vdots \\ \mathbf{\Psi}_{m1} & \cdots & \mathbf{\Psi}_{mm} \end{pmatrix}. \tag{8}$$

Note that, in general, $\mathbf{\Psi}_{ij}$ is not the inverse of the corresponding block $\mathbf{C}_{ij}$ in $\mathbf{C}_{\rm tot}$.

The solution for $\mathbf{D}_c$ and $\mathbf{C}_c$ can be easily found by expanding the expression for the total χ^2 of equation (5) as

$$\chi^2 = \mathbf{D}_{tot}^t \Psi_{tot} \mathbf{D}_{tot} - 2\,\mathbf{T}_{tot}^t \Psi_{tot} \mathbf{D}_{tot} + \mathbf{T}_{tot}^t \Psi_{tot} \mathbf{T}_{tot}. \quad (9)$$

Equivalently, for the consensus values, we will have

$$\chi^2 = \mathbf{D}_c^t \Psi_c \mathbf{D}_c - 2\,\mathbf{T}^t \Psi_c \mathbf{D}_c + \mathbf{T}^t \Psi_c \mathbf{T}. \quad (10)$$

Equating the last terms of equations (9) and (10), we find a general expression for $\mathbf{C}_c$ as

$$\mathbf{C}_c \equiv \Psi_c^{-1} \equiv \left(\sum_{i=1}^{m} \sum_{j=1}^{m} \Psi_{ij} \right)^{-1}, \quad (11)$$

whereas equating the second terms gives the solution for $\mathbf{D}_c$ as

$$\mathbf{D}_c = \Psi_c^{-1} \sum_{i=1}^{m} \left(\sum_{j=1}^{m} \Psi_{ji} \right) \mathbf{D}_i. \quad (12)$$

It is easy to see that in the case in which the different estimates are independent, these expressions reduce to the known formulae

$$\Psi_c = \sum_{i=1}^{m} \Psi_{ii} \quad (13)$$

and

$$\mathbf{D}_c = \Psi_c^{-1} \sum_{i=1}^{m} \Psi_{ii} \mathbf{D}_i, \quad (14)$$

where $\mathbf{\Psi}_{ii}$ corresponds to the precision matrix of measurement i.

Another interesting particular case is when the goal is to obtain the consensus value of a single parameter (i.e. $p = 1$), given a set of m measurements D_i. In this case, equations (11) and (12) show that the consensus mean and dispersion for this parameter will be given by

$$D_c = \sigma_c^2 \sum_{i=1}^{m} \sum_{j=1}^{m} \psi_{ij} D_i \quad (15)$$

and

$$\sigma_c^2 = \left(\sum_{i=1}^{m} \sum_{j=1}^{m} \psi_{ij} \right)^{-1}, \quad (16)$$

which correspond to the result found by Winkler (1981).

2.2 The combination of posterior distributions with different parameters

In certain cases, it might be necessary to combine two or more posterior distributions with different parameters. This situation is encountered, for example, when combining cosmological distance measurements obtained from BAO-only analyses with the information obtained from full-shape fits to anisotropic clustering measurements, which also constrain the growth-rate parameter combination $f\sigma_8(z)$.

The recipe described in the previous section can also be applied in this case. As an example, let us consider the case in which the first data set gives constraints on the first $p - 1$ parameters only, with an associated $(p - 1) \times (p - 1)$ covariance matrix $\tilde{\mathbf{C}}_{11}$. These results can be considered as including a constraint on the remaining parameter, but with an infinite uncertainty, that is,

$$\mathbf{C}_{11} = \begin{pmatrix} \tilde{\mathbf{C}}_{11} & 0 \\ 0 & \infty \end{pmatrix}. \quad (17)$$

In the remaining blocks of the total covariance matrix $\mathbf{C}_{tot}$, the rows and columns corresponding to the undetermined parameter will be zero. This structure will be inherited by the total precision matrix, where also the diagonal entry corresponding to this parameter will cancel. It is then possible to apply the solution of equations (11) and (12) to find the final consensus values that combine all measurements.

In a more general situation, given a set of measurements of different parameter spaces, it is possible to apply the general recipe described here to obtain consensus values on the parameter space defined by the union of those of the individual measurements.

3 APPLICATION TO BAO AND RSD MEASUREMENTS FROM THE BOSS

As an illustration of the procedure described in the previous section, we have applied it to combine the information obtained from a set of cosmological measurements made on the MD-Patchy mock galaxy catalogues (Kitaura et al. 2016), which are designed to mimic the BOSS DR12 sample. These mocks are based on the Patchy recipe of Kitaura, Yepes & Prada (2014), in which dark matter density and velocity fields are generated using augmented Lagrangian perturbation theory (Kitaura & Heß 2013). The initial conditions of the MD-Patchy mock catalogues are based on the same cosmological model as the Big-MultiDark N-body simulations (Klypin et al. 2014), corresponding to the best-fitting ΛCDM cosmology to the *Planck* 2013 cosmic microwave background (CMB) measurements (Planck Collaboration XVI 2014). The halo density field is then modelled using perturbation theory and non-linear stochastic biasing with parameters calibrated against the Big-MultiDark simulations, as described in Rodríguez-Torres et al. (2016). These haloes are populated with galaxies by abundance matching between the DR12 combined sample and the simulations using Hadron (Zhao et al. 2015). The full survey selection is applied to a light-cone built by interpolating the galaxy positions at 10 different intermediate redshifts. The final mock catalogues correctly reproduce the DR12 two- and three-point statistics (Kitaura et al. 2016). From the total set of 2045 mock catalogues produced, we use 996 in our analysis. We followed Alam et al. (2016) and divided each mock catalogue into three overlapping redshift bins of roughly equal effective volume, defined by $0.2 < z < 0.5$, $0.4 < z < 0.6$ and $0.5 < z < 0.75$. We focus first on the combination of the results of the BAO-only and full-shape fits separately and then combine these constraints into a final set of consensus values.

3.1 Post-reconstruction BAO-only fits

The cosmological information encoded in the BAO signal can be expressed in terms of the geometric parameters $D_M(z)/r_d$ and $H(z) \times r_d$. In this section, we focus on the combination of measurements of these quantities derived from BAO-only analyses. For this, we applied the reconstruction algorithm (Eisenstein et al. 2007; Padmanabhan et al. 2012) as described in Cuesta et al. (2016) to each MD-Patchy mock catalogue. This procedure approximately recovers the linear density field, enhancing in this way the significance of the BAO signal in our clustering measurements.

For each mock catalogue, we then applied the methodologies of Ross et al. (2016) and Beutler et al. (2016b) to perform BAO-only fits in each of our three redshift bins. We now present a brief description of the methodologies used in these analyses and refer the reader to those papers for more details.

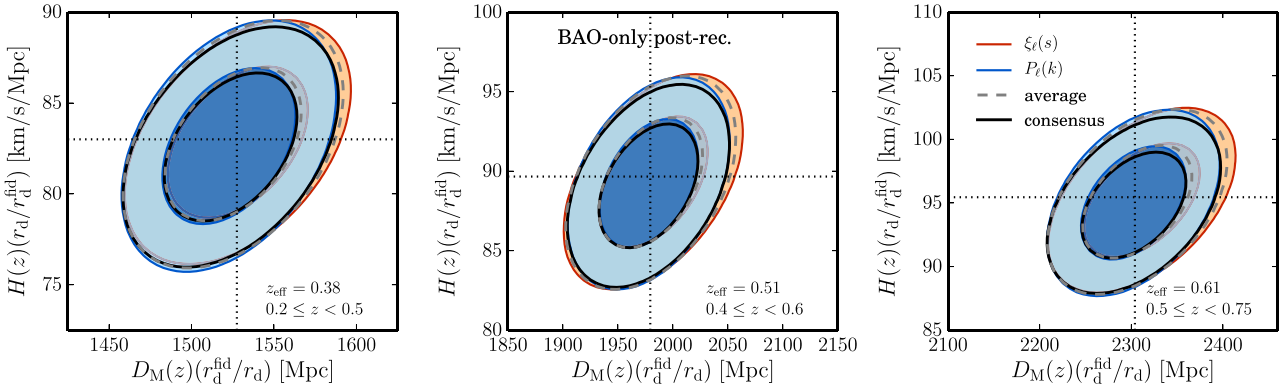

Figure 1. The mean 68 and 95 per cent two-dimensional constraints on the parameters $D_{\rm M}(z)(r_{\rm d}^{\rm fid}/r_{\rm d})$ and $H(z)(r_{\rm d}/r_{\rm d}^{\rm fid})$ obtained by applying the BAO-only analyses of Ross et al. (2016, orange) and Beutler et al. (2016b, blue) to 996 MD-Patchy BOSS mock catalogues for the redshift bins indicated in the legend. The results are in excellent agreement with the true underlying values of these parameters, indicated by the dotted lines. The full information from these measurements can be combined into a set of consensus constraints (black solid lines), as described in Section 2. The dashed lines correspond to the combination of the results obtained by averaging the logarithm of the two posterior distributions.

Ross et al. (2016) use the information of the post-reconstruction correlation function multipoles of order $\ell = 0, 2$ for scales $20 < s < 180\,h^{-1}$ Mpc. The methodology employed in this analysis follows that of Xu et al. (2015), Anderson et al. (2014b) and Ross et al. (2015) and is based on templates of $\xi_{0,2}(s)$ that are constructed for the fiducial cosmology (i.e. the cosmology assumed when obtaining the clustering measurements). To account for the Alcock–Paczynski distortions (Alcock & Paczynski 1979), the BAO features in these templates are altered as a function of the relative change in $D_{\rm M}(z)$ and $H(z)$ with respect to those of the fiducial cosmology. To isolate the signal of the anisotropic BAO feature, these templates are also allowed to vary in amplitude and are combined with third-order polynomials that marginalize over any shape information.

Beutler et al. (2016b) extract the BAO information from the power spectrum multipoles $P_{0,2}(k)$ measured using the fast Fourier transform based estimator proposed by Bianchi, Percival & Bel (2015) and Scoccimarro (2015). The methodology used to extract the BAO signal is based on that of Seo et al. (2016). A model for the full anisotropic power spectrum is constructed by combining a smooth component describing its broad-band features and an oscillating one that accounts for the BAO signal. This model is used to construct theoretical predictions for the multipoles $P_\ell(k)$ for scales $k < 0.3\,h\,{\rm Mpc}^{-1}$, which are convolved with the window function of the survey and combined with third-order polynomials in an analogous way as the configuration-space analysis.

Fig. 1 shows the mean two-dimensional constraints on $D_{\rm M}(z)/r_{\rm d}$ and $H(z) \times r_{\rm d}$ for each redshift bin, rescaled by the sound horizon at the drag redshift for our fiducial cosmology, $r_{\rm d}^{\rm fid} = 147.78$ Mpc, to express them in units of Mpc and km s^{-1} Mpc^{-1}. The results inferred from the configuration and Fourier-space analyses are completely consistent and in excellent agreement with the true underlying values of these parameters, which are shown by the dotted lines. This indicates that both methods are able to extract essentially the same information from the clustering measurements. However, the results obtained from each set of measurements on individual mock catalogues are affected by noise in different ways. This can be seen in Fig. 2, which shows scatter plots of the two sets of constraints obtained from each mock catalogue for our intermediate-redshift bin. Although they are highly correlated, the correlation coefficients between the results derived from the two methods are not exactly one, which means that additional information can be obtained by combining them.

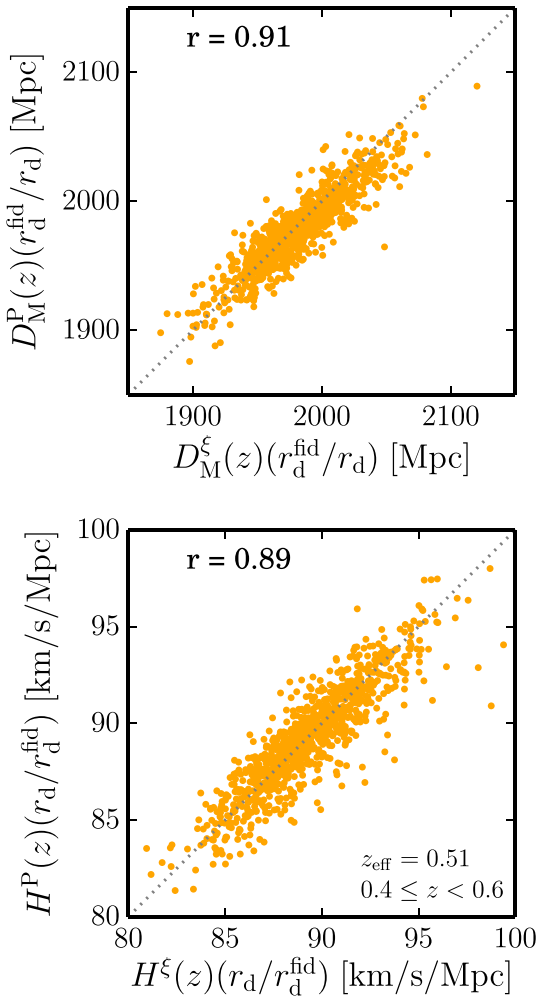

Figure 2. Scatter plots of the BAO-only constraints on $D_{\rm M}(z)(r_{\rm d}^{\rm fid}/r_{\rm d})$ and $H(z)(r_{\rm d}/r_{\rm d}^{\rm fid})$ obtained from the configuration and Fourier-space BAO-only analyses of 996 MD-Patchy mock catalogues for $0.4 < z < 0.6$. Although the results obtained from these methods are highly correlated, their correlation coefficients, r, are not exactly one, indicating that additional information can be obtained from their combination.

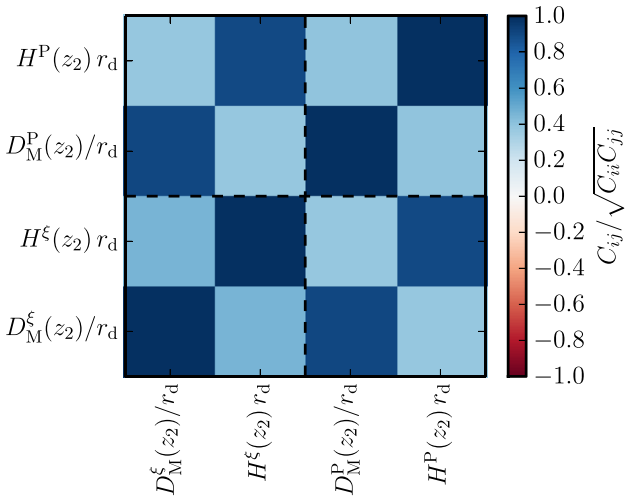

Figure 3. Correlation matrix corresponding to the full covariance $\mathbf{C}_{\rm tot}$ of the BAO-only constraints on $D_{\rm M}(z)/r_{\rm d}$, and $H(z) \times r_{\rm d}$, constructed from the individual MD-Patchy mock catalogues in configuration and Fourier space. The blocks $\mathbf{C}_{ij}$ indicated by the dashed lines correspond to the auto- and cross-covariance matrices of the two methods.

The results obtained from the two methods on each individual mock catalogue can be used to construct the total covariance matrix $\mathbf{C}_{\rm tot}$. As an example, Fig. 3 shows the normalized correlation matrix corresponding to the results of the intermediate-redshift bin. The dashed lines divide the matrix into the blocks associated with $\mathbf{C}_{ij}$. Due to the high correlation between the results of the power spectrum and correlation function fits, the structure of the off-diagonal block $\mathbf{C}_{12}$ is very similar to that of the auto-covariances. Inverting the matrix $\mathbf{C}_{\rm tot}$ to obtain the total precision matrix $\Psi_{\rm tot}$ and using equations (11) and (12), the results of both methods can be combined into sets of consensus constraints for each redshift bin, which are shown by the black solid lines in Fig. 1. As described in Section 2, these constraints contain the joint information of the two sets of results.

Anderson et al. (2012, 2014a,b) derived consensus anisotropic BAO constraints from the combination of the results inferred from the analysis of the Legendre multipoles of the correlation function and clustering wedges statistic (Kazin et al. 2012). These consensus constraints were computed by averaging the logarithm of the two-dimensional posterior distributions on $D_{\rm M}(z)/r_{\rm d}$ and $H(z) \times r_{\rm d}$ obtained from each method:

$$\ln P_{\rm c} = \frac{1}{m}\sum_{i=1}^{m} \ln P_i . \tag{18}$$

The dashed lines in Fig. 1 show the result of applying this procedure to the constraints inferred from the Fourier- and configuration-space fits to our mock catalogues. As the original distributions are similar, their average is also in agreement with the full consensus constraints but results in a slightly larger allowed region for $D_{\rm M}(z)/r_{\rm d}$ and $H(z) \times r_{\rm d}$. This difference can be quantified in terms of the figure of merit, FoM, given by

$$\mathrm{FoM} = (\det[\mathbf{C}])^{-1/2} . \tag{19}$$

The FoM values of the consensus constraints are larger than those of the average profile by a factor of 1.07, 1.08 and 1.10 for the low-, intermediate- and high-redshift bins, respectively. As we will see in the following sections, this is a common feature of the result of the average profile.

3.2 Pre-reconstruction full-shape fits

In this section, we focus on the combination of the results inferred from full-shape fits (which we refer to as BAO+RSD analyses) to various pre-reconstruction anisotropic clustering measurements. Using the information encoded in the full shape of these measurements, it is possible to constrain the same geometric parameters as the BAO-only studies, $D_{\rm M}(z)/r_{\rm d}$ and $H(z) \times r_{\rm d}$, and the growth rate of cosmic structure, characterized by the combination $f\sigma_8(z)$, where

$$f = \frac{{\rm d}\ln D}{{\rm d}\ln a} \tag{20}$$

is the logarithmic derivative of the growth factor. We consider the analysis methods applied to the final BOSS data in our companion papers (Beutler et al. 2016a; Grieb et al. 2016; Sánchez et al. 2016; Satpathy et al. 2016), which we briefly summarize below.

Satpathy et al. (2016) fit the full shape of the monopole and quadrupole of the two-point correlation function for scales between 25 and 150 h^{-1} Mpc by using a model based on convolution Lagrangian perturbation theory (Carlson, Reid & White 2013; Wang, Reid & White 2014) and the Gaussian streaming model (Scoccimarro 2004; Reid & White 2011). Sánchez et al. (2016) use a new model of the non-linear evolution of density fluctuations (Crocce, Blas & Scoccimarro, in preparation) and RSD (Scoccimarro, in preparation) to extract cosmological information from the full shape of three clustering wedges in configuration space, $\xi_{3{\rm w}}(s)$, for scales s between 20 and 160 h^{-1} Mpc.

Beutler et al. (2016a) apply a model based on Taruya, Nishimichi & Saito (2010) to the power spectrum multipoles $P_\ell(k)$, for $\ell = 0$, 2, 4, up to scales of $k = 0.15\,h\,{\rm Mpc}^{-1}$ for the monopole and quadrupole, and $k = 0.1\,h\,{\rm Mpc}^{-1}$ for the hexadecapole. The analysis of Grieb et al. (2016) is based on measurements of three power spectrum wedges, $P_{3{\rm w}}(k)$, obtained by filtering out the information of Legendre multipoles $\ell > 4$, for scales $k < 0.2\,h\,{\rm Mpc}^{-1}$. These measurements are fitted with theoretical predictions based on the same model as the configuration-space analysis of Sánchez et al. (2016). All Fourier-space analyses require an accurate description of the impact of the window function of the survey on the power spectrum measurements, which for these analyses was based on the recipe of Beutler et al. (2014).

These different analysis methodologies have been validated using the results of N-body simulations and mock catalogues and found to give accurate cosmological constraints without introducing any significant systematic errors (Tinker et al., in preparation). We applied these methods to each of our mock catalogues in the same way as they were applied to the real BOSS data. Fig. 4 shows the mean 68 and 95 per cent confidence level constraints on $D_{\rm M}(z)/r_{\rm d}$, $H(z) \times r_{\rm d}$ and $f\sigma_8(z)$ of the results inferred from each individual mock catalogue for our intermediate-redshift bin. The filled contours correspond to the results obtained from the correlation function multipoles $\xi_{0,\,2}(s)$ (magenta), the power spectrum multipoles $P_{0,\,2,\,4}(k)$ (blue), the correlation function wedges $\xi_{3{\rm w}}(s)$ (orange) and the power spectrum wedges $P_{3{\rm w}}(k)$ (green). The results obtained from these measurements are completely consistent and in good agreement with the correct values for the cosmology of the mock catalogues, shown by the dotted lines. However, the different measurements and range of scales included in each analysis, as well as the models applied to these data, lead to results with larger differences than in the BAO-only case. We used the methodology described in Section 2 to obtain a set of consensus values representing the joint information from these analyses.

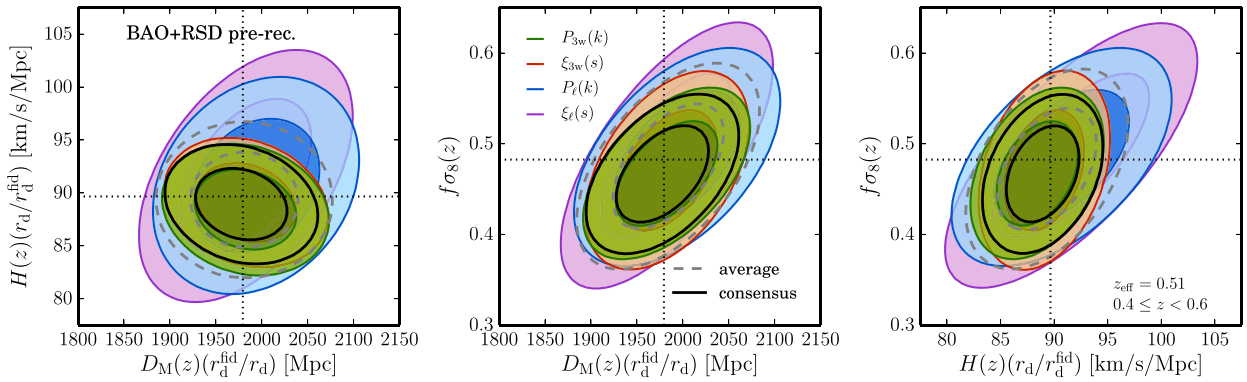

Figure 4. The mean 68 and 95 per cent two-dimensional constraints on the parameters $D_{\rm M}(z)(r_{\rm d}^{\rm fid}/r_{\rm d})$, $H(z)(r_{\rm d}/r_{\rm d}^{\rm fid})$ and $f\sigma_8(z)$ inferred from our mock BOSS catalogues for $0.4 < z < 0.6$. The filled contours correspond to the results obtained by means of full-shape fits of the Legendre multipoles, $\xi_\ell(s)$ (magenta) and $P_\ell(k)$ (blue) and clustering wedges $\xi_{3w}(s)$ (orange) and $P_{3w}(k)$ (green), using the methodology of our companion papers (Beutler et al. 2016a; Grieb et al. 2016; Sánchez et al. 2016; Satpathy et al. 2016). The obtained constraints are in good agreement with the true underlying values of these parameters, indicated by the dotted lines. The black solid contours correspond to the combination of these measurements into a set of consensus constraints, computed as described in Section 2. The dashed lines correspond to the combination of the results obtained by averaging the logarithms of the four posterior distributions.

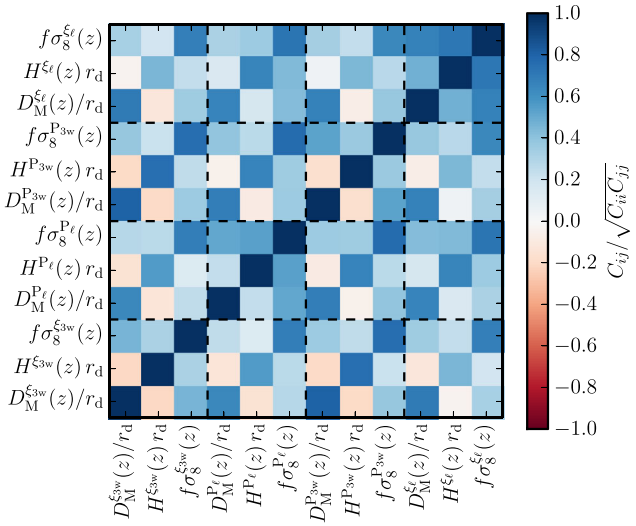

Figure 5. Correlation matrix corresponding to the total covariance $\mathbf{C}_{\rm tot}$ of the full-shape fits of the Legendre multipoles and clustering wedges in configuration and Fourier space constructed from the individual MD-Patchy mock catalogues. The blocks $\mathbf{C}_{ij}$ indicated by the dashed lines correspond to the auto- and cross-covariance matrices of the different methods.

We used the results obtained from the application of the different methods to our mock catalogues to construct the full covariance matrices $\mathbf{C}_{\rm tot}$ in our three redshift bins. As an example, Fig. 5 shows the corresponding correlation matrix for the intermediate-redshift bin. The dashed lines divide the matrix into the blocks $\mathbf{C}_{ij}$, corresponding to the auto- and cross-covariance matrices of the methods. The different estimates of each parameter are highly correlated. The differences between the methods are also reflected in the structure of the correlation matrix, which is more complicated than for the BAO-only case.

We used equations (11) and (12) to derive consensus constraints for each mock catalogue. The back solid contours in Fig. 4 correspond to the mean consensus constraints. As the consensus results combine the information of all four measurements, they provide tighter constraints than each of them individually. This highlights the gain obtained from the combination of the methods, with respect to the individual analyses.

The grey dashed lines in the same figure correspond to the results obtained by averaging the logarithm of the posterior distributions recovered from the different methods. The difference between these constraints and the consensus values can be quantified by extending the definition of the FoM from equation (19) to the three-dimensional covariance matrices of the consensus and average constraints. In this case, the FoM values of the consensus constraints are larger than those of the average profile by a factor of $\backsim$2.5 in all redshift bins. This difference clearly shows that the average profile does not reproduce the full information of the different estimates.

3.3 Final consensus constraints

In this section, we focus on the combination of the consensus BAO-only constraints derived in Section 3.1, which are sensitive only to the geometric quantities $D_{\rm M}(z)/r_{\rm d}$ and $H(z) \times r_{\rm d}$, with those of the full-shape BAO+RSD measurements derived in Section 3.2, which also include $f\sigma_8(z)$. As these posterior distributions contain different parameters, we proceed as described in Section 2.2 and interpret the BAO-only results as providing an estimate of $f\sigma_8(z)$ with infinite uncertainty. The blue and green contours of Fig. 6 show the consensus constraints on our intermediate-redshift bin for the BAO-only and BAO+RSD cases, respectively. As can be seen in the left-hand panel, the constraints in the $D_{\rm M}(z)/r_{\rm d}$–$H(z) \times r_{\rm d}$ plane follow different correlations, which suggests that their combination could lead to a significant improvement of the constraints.

We used the BAO-only and BAO+RSD consensus values inferred from each mock catalogue in Sections 3.1 and 3.2 to obtain the covariance matrix $\mathbf{C}_{\rm tot}$ associated with these constraints. Fig. 7 shows the associated correlation matrix, wherein the diagonal entry corresponding to the BAO-only estimate of $f\sigma_8(z)$ is undetermined (shown in grey), and its corresponding row and column are set to zero. This structure is repeated in the total precision matrix $\Psi_{\rm tot}$ but with the corresponding diagonal entry also set to zero. The application of equations (11) and (12) leads to a final set of consensus constraints, encoding the full information of the BAO-only and BAO+RSD analyses. The results corresponding to the intermediate-redshift bin are shown by the filled contours in Fig. 7, wherein the reduction in the allowed region of the parameter space with respect to the BAO and RSD results is clear.

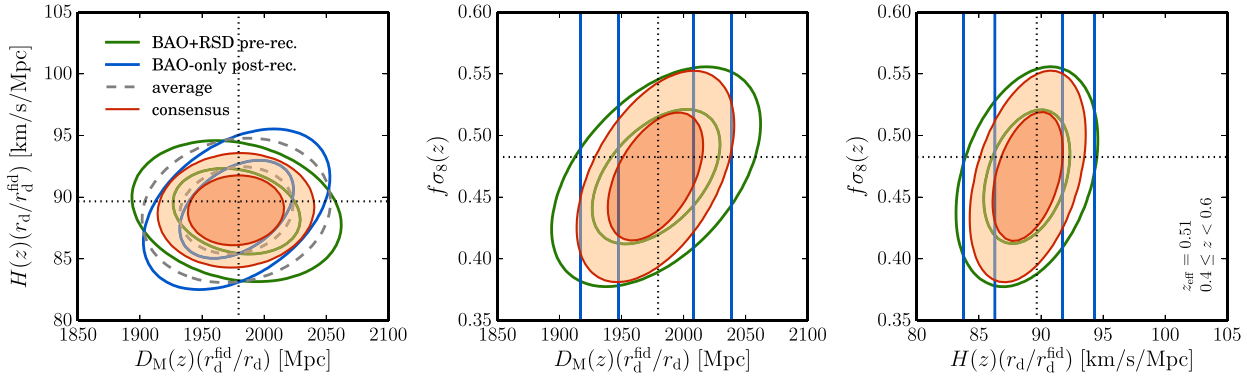

Figure 6. The mean 68 and 95 per cent two-dimensional consensus constraints on the parameters $D_\mathrm{M}(z)(r_\mathrm{d}^\mathrm{fid}/r_\mathrm{d})$, $H(z)(r_\mathrm{d}/r_\mathrm{d}^\mathrm{fid})$ and $f\sigma_8(z)$ inferred from our mock BOSS catalogues for $0.4 < z < 0.6$. The blue and green contours correspond to the combination of the BAO-only and full-shape BAO+RSD fits, respectively. The dotted lines indicate the correct values of these parameters. The filled contours correspond to the combination of these results into a final set of consensus constraints, containing the joint information of the two sets of measurements. The dashed contours in the left-hand panel correspond to the result obtained by averaging the logarithms of the two posterior distributions.

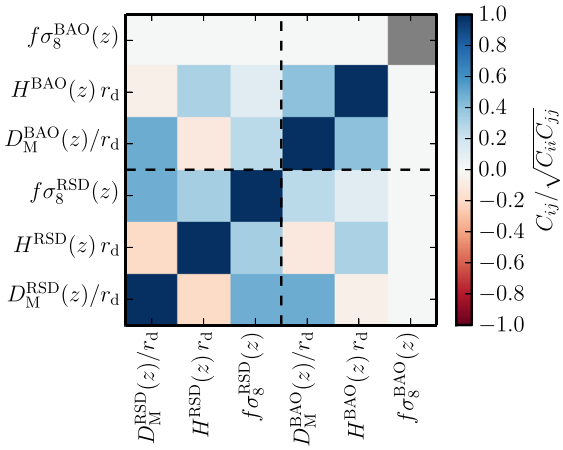

Figure 7. Correlation matrix corresponding to the joint covariance $\mathbf{C}_\mathrm{tot}$ of the BAO-only and full-shape consensus results derived in Sections 3.1 and 3.2. The dashed lines indicate the blocks $\mathbf{C}_{ij}$ corresponding to the auto- and cross-covariance matrices of the two methods. As BAO-only measurements cannot constrain the value of $f\sigma_8(z)$, the corresponding diagonal entry is undetermined (shown in grey), and its row and column are set to zero.

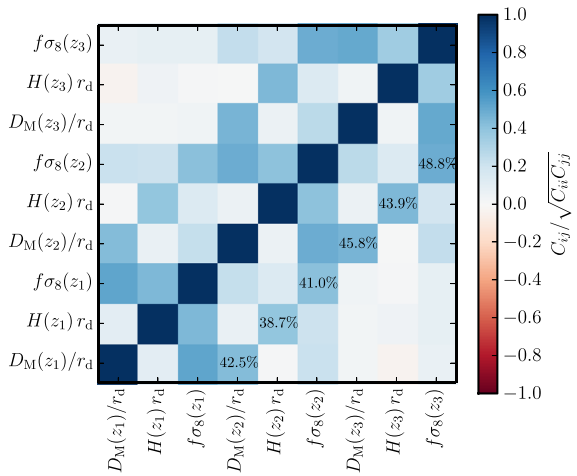

Figure 8. Correlation matrix corresponding to the covariance of the full consensus constraints in our three redshift bins recovered from our BOSS mock catalogues.

Fig. 8 shows the correlation matrix corresponding to the covariance of the full consensus constraints recovered from our BOSS mock catalogues in the three redshift bins. The 3×3 blocks along the diagonal correspond to the consensus covariance $\mathbf{C}_\mathrm{c}$ at each redshift, which shows a similar structure. As can be seen from the off-diagonal blocks, the consensus constraints of the low- and high-redshift bins are essentially independent, but both exhibit a strong correlation with the results of the intermediate one due to the large redshift overlap. Alam et al. (2016) use this covariance matrix as the basis of the cosmological implications of the consensus constraints combining the results of the same BAO-only and BAO+RSD methods studied here.

So far we have assumed that the posterior distributions being combined are not affected by systematic errors. If they are, these errors will be propagated into the consensus values and might lead to biased cosmological constraints. If the different methods are affected by uncorrelated systematic errors, their impact on the consensus results would be reduced. However, if these systematic errors shift the value of a given parameter from the correct result always in the same direction, this deviation will also be presented in the combined constraints. The methodologies implemented here to extract cosmological information from BAO+RSD fits show a small deviation from the correct value of $f\sigma_8(z)$ in the low- and intermediate-redshift bins. These shifts are inherited by the final consensus constraints, which show a deviation from the true value of 0.59, 0.42 and 0.06σ for the low-, intermediate- and high-redshift bins, respectively. Although these systematic shifts are smaller than the statistical uncertainties associated with the consensus constraints, they are taken into account in Alam et al. (2016), wherein they are used to construct a systematic error budget for the measurements obtained from the final BOSS galaxy samples.

4 CONCLUSIONS

We presented a general framework to combine the information of multiple Gaussian posterior distributions into a set of consensus constraints representing their joint information. This methodology can be applied to combine the cosmological information obtained from different clustering measurements based on the same galaxy sample, which can often be expressed as Gaussian constraints on a small number of parameters. The application of this technique requires the knowledge of the full cross-covariances of the

different methods. For clustering measurements, this information can be obtained using a brute-force approach, applying the same methods being combined to a set of mock galaxy catalogues and measuring the correlations between the obtained results.

We illustrate our technique by applying it to combine the results obtained from different BAO-only and BAO+RSD measurements from an ensemble of mock catalogues of the final BOSS. The obtained consensus constraints represent a reduction in the allowed region of the parameter space with respect to the results of the individual methods. This shows the value of using the combination of the results of multiple clustering analyses as a strategy to maximize the constraining power of galaxy surveys.

In our companion paper Alam et al. (2016), the methodology described here is used to obtain a set of consensus constraints that encode the results obtained by applying the same methods studied here to the final BOSS galaxy samples. These results are then used to explore the cosmological implications of the data set in combination with the information from CMB and Type Ia supernovae data.

We anticipate that the procedure detailed here can help us to optimize the use of the cosmological information encoded in future clustering and lensing analyses.

ACKNOWLEDGEMENTS

AGS would like to thank Ximena Mazzalay for her invaluable help in the preparation of this manuscript. We would like to thank Riccardo Bolze, Daniel Farrow, Jiamin Hou, Martha Lippich and Francesco Montesano for useful discussions. AGS, JNG and SS-A acknowledge support from the Trans-regional Collaborative Research Centre TR33 'The Dark Universe' of the German Research Foundation (DFG). C-HC acknowledges support as a MultiDark Fellow. C-HC also acknowledges support from the Spanish MICINNs Consolider-Ingenio 2010 Programme under grant MultiDark CSD2009-00064, MINECO Centro de Excelencia Severo Ochoa Programme under grant SEV-2012-0249, and grant AYA2014-60641-C2-1-P. MV-M is partially supported by Programa de Apoyo a Proyectos de Investigación e Innovación Tecnológica (PAPITT) No IA102516.

Funding for SDSS-III has been provided by the Alfred P. Sloan Foundation, the Participating Institutions, the National Science Foundation and the U.S. Department of Energy.

SDSS-III is managed by the Astrophysical Research Consortium for the Participating Institutions of the SDSS-III Collaboration, including the University of Arizona, the Brazilian Participation Group, the Brookhaven National Laboratory, the University of Cambridge, Carnegie Mellon University, the University of Florida, the French Participation Group, the German Participation Group, Harvard University, the Instituto de Astrofisica de Canarias, the Michigan State/Notre Dame/JINA Participation Group, The Johns Hopkins University, the Lawrence Berkeley National Laboratory, the Max Planck Institute for Astrophysics, the Max Planck Institute for Extraterrestrial Physics, New Mexico State University, New York University, Ohio State University, Pennsylvania State University, the University of Portsmouth, Princeton University, the Spanish Participation Group, the University of Tokyo, the University of Utah, Vanderbilt University, the University of Virginia, the University of Washington and Yale University.

Based on observations obtained with *Planck* (http://www.esa.int/Planck), an ESA science mission with instruments and contributions directly funded by ESA Member States, NASA, and Canada.

REFERENCES

Alam S. et al., 2016, preprint (arXiv:1607.03155)
Alcock C., Paczynski B., 1979, Nature, 281, 358
Anderson L. et al., 2012, MNRAS, 427, 3435
Anderson L. et al., 2014a, MNRAS, 439, 83
Anderson L. et al., 2014b, MNRAS, 441, 24
Beutler F. et al., 2014, MNRAS, 443, 1065
Beutler F. et al., 2016a, MNRAS, in press
Beutler F. et al., 2016b, preprint (arXiv:1607.03150)
Bianchi D., Gil-Marín H., Ruggeri R., Percival W. J., 2015, MNRAS, 453, L11
Carlson J., Reid B., White M., 2013, MNRAS, 429, 1674
Cole S. et al., 2005, MNRAS, 362, 505
Colless M. et al., 2001, MNRAS, 328, 1039
Colless M. et al., 2003, preprint (astro-ph/0306581)
Cuesta A. J. et al., 2016, MNRAS, 457, 1770
Dawson K. S. et al., 2013, AJ, 145, 10
Dawson K. S. et al., 2016, AJ, 151, 44
Drinkwater M. J. et al., 2010, MNRAS, 401, 1429
Eisenstein D. J. et al., 2005, ApJ, 633, 560
Eisenstein D. J., Seo H.-J., Sirko E., Spergel D. N., 2007, ApJ, 664, 675
Eisenstein D. J. et al., 2011, AJ, 142, 72
Grieb J. N. et al., 2016, preprint (arXiv:1607.03143)
Hill G. et al., 2008, Astronomy Society of the Pacific Conference Series Vol. 399, Astron. Soc. Pac., San Francisco, p. 115
Jones D. H. et al., 2009, MNRAS, 399, 683
Kazin E. A., Sánchez A. G., Blanton M. R., 2012, MNRAS, 419, 3223
Kitaura F.-S., Heß S., 2013, MNRAS, 435, 78
Kitaura F.-S., Yepes G., Prada F., 2014, MNRAS, 439, L21
Kitaura F.-S. et al., 2016, MNRAS, 456, 4156
Klypin A., Yepes G., Gottlöber S., Prada F., Heß S., 2016, MNRAS, 457, 4340
Laureijs R. et al., 2011, preprint (arXiv:1110.3193)
Levi M. et al., 2013, preprint (arXiv:1308.0847)
Padmanabhan N., White M., 2008, Phys. Rev. D, 77, 123540
Padmanabhan N., Xu X., Eisenstein D. J., Scalzo R., Cuesta A. J., Mehta K. T., Kazin E., 2012, MNRAS, 427, 2132
Planck Collaboration XVI, 2014, A&A, 571, 16
Reid B. A., White M., 2011, MNRAS, 417, 1913
Rodríguez-Torres S. A. et al., 2016, MNRAS, 460, 1173
Ross A. J., Samushia L., Howlett C., Percival W. J., Burden A., Manera M., 2015, MNRAS, 449, 835
Ross A. J. et al., 2016, MNRAS, 464, 1168
Sánchez A. G. et al., 2016, MNRAS, in press
Satpathy S. et al., 2016, preprint (arXiv:1607.03148)
Scoccimarro R., 2004, Phys. Rev. D, 70, 083007
Scoccimarro R., 2015, Phys. Rev. D, 92, 083532
Seo H.-J., Beutler F., Ross A. J., Saito S., 2016, MNRAS, 460, 2453
Taruya A., Nishimichi T., Saito S., 2010, Phys. Rev. D, 82, 063522
Tegmark M. et al., 2004, ApJ, 606, 702
Wang L., Reid B., White M., 2014, MNRAS, 437, 588
Winkler R. L., 1981, Manage. Sci., 27, 479
Xu X., Padmanabhan N., Eisenstein D. J., Mehta K. T., Cuesta A. J., 2015, MNRAS, 427, 2146
Zhao C., Kitaura F.-S., Chuang C.-H., Prada F., Yepes G., Tao C., 2015, MNRAS, 451, 4266

[1]*Max-Planck-Institut für extraterrestrische Physik, Postfach 1312, Giessenbachstrasse 1, D-85741 Garching, Germany*
[2]*Universitäts-Sternwarte München, Ludwig-Maximilians-Universität München, Scheinerstrasse 1, D-81679 Munich, Germany*
[3]*Department of Physics, Carnegie Mellon University, 5000 Forbes Avenue, Pittsburgh, PA 15217, USA*
[4]*McWilliams Center for Cosmology, Carnegie Mellon University, 5000 Forbes Avenue, Pittsburgh, PA 15217, USA*

[5]*Institute of Cosmology & Gravitation, University of Portsmouth, Dennis Sciama Building, Portsmouth PO1 3FX, UK*
[6]*Lawrence Berkeley National Laboratory, 1 Cyclotron Road, Berkeley, CA 94720, USA*
[7]*Center for Cosmology and Astro-Particle Physics, Ohio State University, Columbus, OH 43210, USA*
[8]*Department of Physics and Astronomy, University of Utah, 115 S 1400 E, Salt Lake City, UT 84112, USA*
[9]*Instituto de Física Teórica, (UAM/CSIC), Universidad Autónoma de Madrid, Cantoblanco, E-28049 Madrid, Spain*
[10]*Leibniz-Institut für Astrophysik Potsdam (AIP), An der Sternwarte 16, D-14482 Potsdam, Germany*
[11]*Institut de Ciències del Cosmos (ICCUB), Universitat de Barcelona (IEEC-UB), Martí i Franquès 1, E-08028 Barcelona, Spain*
[12]*Harvard–Smithsonian Center for Astrophysics, 60 Garden Street, Cambridge, MA 02138, USA*
[13]*Departments of Physics and Astronomy, University of California, Berkeley, CA 94720, USA*
[14]*Campus of International Excellence UAM+CSIC, Cantoblanco, E-28049 Madrid, Spain*
[15]*Instituto de Astrofísica de Andalucía (CSIC), Glorieta de la Astronomía, E-18080 Granada, Spain*
[16]*Departamento de Física Teórica, Universidad Autónoma de Madrid, Cantoblanco, E-28049 Madrid, Spain*
[17]*Department of Physics and Astronomy, Ohio University, 251B Clippinger Labs, Athens, OH 45701, USA*
[18]*Center for Cosmology and Particle Physics, New York University, New York, NY 10003, USA*
[19]*School of Physics and Astronomy, University of St Andrews, North Haugh, St Andrews KY16 9SS, UK*
[20]*Instituto de Fisica, Universidad Nacional Autónoma de México, Apartado Postal 20-364, 01000 México D.F., Mexico*
[21]*Brookhaven National Laboratory, Building 510, Upton, NY 11973, USA*
[22]*National Astronomy Observatories, Chinese Academy of Science, Beijing 100012, P.R. China*

This paper has been typeset from a TEX/LATEX file prepared by the author.